 doi:10.20944/preprints201610.0074.v1

Article

Novel Step-up DC-to-DC Converter with Isolated Transformer and Switched-Clamp Capacitor Techniques for Renewable Systems

Yong-Seng Wong [1,2], Jiann-Fuh Chen [1,*] and Kuo-Bin Liu [2]

[1] Department of Electrical Engineering, National Cheng Kung University, No. 1 University Road, Tainan 701, Taiwan; wong.ys@nsrrc.org.tw
[2] Power Supply Group, National Synchrotron Radiation Research Center, 101, Hsin-Ann Rd., Hsinchu 300, Taiwan; kbl@nsrrc.org.tw
* Correspondence: chenjf@mail.ncku.edu.tw; Tel.: +886-6-275-7575 (ext. 62353)

Abstract: A high step-up DC-to-DC converter that integrates an isolated transformer and a switched-clamp capacitor is presented in this study. The voltage stress of the main power switch should be clamped to 1/4 *V* by using the turn ratio and switched-clamp capacitor of an isolated transformer to achieve a high voltage gain. In addition, a passive clamp circuit is employed reduce voltage stress on the main power switch. The energy of the leakage inductor can be recycled by the clamp capacitor because of the passive clamp circuit, thereby improving the power converter efficiency. The converter consists of one isolated transformer, one main switch, three capacitors, and four diodes. Operating principle and steady-state analyses are also discussed. Finally, a 24-V-input voltage to 200-V-output voltage and a 150 W output power prototype converter are fabricated in the laboratory. The maximum efficiency of the converter is 95.1 at 60 W.

Keywords: high voltage gain; switch-clamp capacitor; DC–DC converter; renewable energy

1. Introduction

In the 21st century, the rapid industrial development has caused severe environmental pollution. The extent of damage to the environment has become irreparable. To obtain power and energy, substantial natural resources have been depleting because of massive exploitation of oil and natural gases. In particular, severe air pollution has been caused by coal combustion. In view of this phenomenon, a number of recommendations had been proposed in the 2015 Paris United Nations Climate Change Conference (i.e., COP21 or CMP11) to cope with the changing climate, as follows: (1) The global average temperature should be controlled within 2 °C of the pre-industrial temperature, and (2) the universal availability of sustainable energy should be promoted in developing countries to strengthen the use of renewable energy sources [1]. Therefore, renewable energy technologies are being investigated, focusing on developing a new high step-up circuit architecture and using renewable energy as the main power source through direct current (DC) to alternating current (AC) inverter technology [2]–[4]. The current mainstream renewable energy sources are wind and solar energies. The proposed renewable energy output voltage has a low-voltage system that requires high step-up circuits to be converted to high output voltage systems [5]–[7]. A simple but highly efficient circuit structure should be designed to comply with the security rules of the isolation circuit architecture [8].

The National Synchrotron Radiation Research Center of Taiwan costs $100 million. The solar modules from TYNSOLAR Co., Ltd. comprise a single photovoltaic module that can reach a maximum power of 150 W and a maximum input voltage of 24 V. In this study, a group of high step-up circuits were developed within the TYNSOLAR photovoltaic module group of the converter.

 doi:10.20944/preprints201610.0074.v1

Several basic circuits, such as the boost and flyback converters, can take high step-up voltage gains for extreme duty cycles. However, high step-up gain is limited by the capacitor, inductor main power switch, and resistance, because electromagnetic interference and reverse-recovery issues are encountered at extreme duty cycles. Moreover, the leakage inductor of the transformer will cause high power dissipation and high voltage spikes on the main power switch. Therefore, a main power switch with high stress voltage must be selected because of excessive cost and space issues.

Many topologies of high step-up converters have been proposed, including coupled inductor technology [9]–[12], switched-clamp capacitor technology [13]–[15], and isolated transformer technology [16]–[19]. Coupled inductor technology can cause substantial leakage inductance. A snubber circuit can absorb leaked energy; however, the circuit efficiency may be reduced. A switched-clamp capacitor can store energy when the switch is turned on. When the power is switched off after, the energy in the capacitor is delivered to the output loading. However, the electric system prevents current flow and no direct conduction path is permitted. As a result, the isolated transformer technology has been proposed to meet the safety standards of galvanic isolation [20]. This technique can easily achieve a high output voltage that uses turn ratio to achieve high voltage gain. The technology can be set to the required voltage by adjusting the turn ratio and duty cycle. An isolated step-up DC–DC converter is suitable as a renewable energy source in low-output-voltage systems. Moreover, this converter can produce high voltage output and achieve isolation. However, an isolated transformer can also produce leakage inductance; thus, a clamp circuit is necessary to recycle energy and achieve high efficiency [21]–[25].

In this study, a high step-up and high efficiency DC–DC converter is proposed. The input source is photovoltaic renewable energy, which is transferred to output loading through the proposed high step-up DC–DC converter circuit. The use of a clamp circuit can prevent spikes and clamping voltage stresses on the switch. When choosing switching elements, selecting low $R_{ds(on)}$ components can reduce conduction losses. An isolated transformer can be viewed as a forward converter that transfers energy to the secondary side when the switch is turned on. At the same time, the switched-clamp and clamp circuit capacitors also transfer energy to the loading. When the switch is turned off, the clamp circuit absorbs the energy stored in the leakage inductance, whereas the switched-clamp capacitor can store energy from the primary side. The proposed circuit architecture can achieve a step-up output voltage through duty cycle modulation. Moreover, the passive clamp circuit can obtain recycled energy, and the clamping voltage stress on the switch can facilitate a high efficiency power converter.

The features of the proposed converter are as follows:

(1) satisfies the safety standards for galvanic isolation;
(2) small isolated transformer;
(3) high step-up voltage gain;
(4) recycles leakage inductor energy and clamps voltage stress on the main switch through the passive clamp circuit;
(5) high efficiency.

2. Operation Principle of the Proposed Converter

For the proposed converter, an integrated switched-clamp capacitor and isolated transformer can achieve high voltage gain and clamp spike voltage on the main power switch. However, the proposed converter needs a highly effective capacitor C_1 and diodes D_1 and D_2. This section details the operating modes at continuous conduction mode (CCM) and discontinuous conduction mode (DCM) during a switching period.

Fig. 1 illustrates the proposed converter structure. The proposed converter circuit consists of isolated transformers N_p and N_s, the main power switch S, and a secondary side step-up circuit that has diodes D_3 and D_4 and capacitor C_2. The clamp circuit has diodes D_1 and D_2, capacitor C_1, and large output capacitors C_{o1} and C_{o2}. The leakage inductor energy loss is recycled by a passive clamp circuit capacitor C_1 that clamps the voltage stress on the main switch.

Preprints (www.preprints.org) | NOT PEER-REVIEWED | Posted: 18 October 2016 doi:10.20944/preprints201610.0074.v1

Before discussing the circuit operation principles, the following conditions were assumed to simplify the analysis of the proposed converter:

(1) Capacitors C_1, C_2, C_{o1}, and C_{o2} are sufficiently large. Thus, V_{C1}, V_{C2}, V_{Co1}, and V_{Co2} are constant during operation.
(2) The parasitic capacitor of power devices is not neglected.
(3) The coupling coefficient is defined as k, which is equal to $L_m/(L_m + L_k)$. The magnetizing inductance is L_m and the leakage inductance is L_k.
(4) Turn ratio n is equal to N_s/N_p.

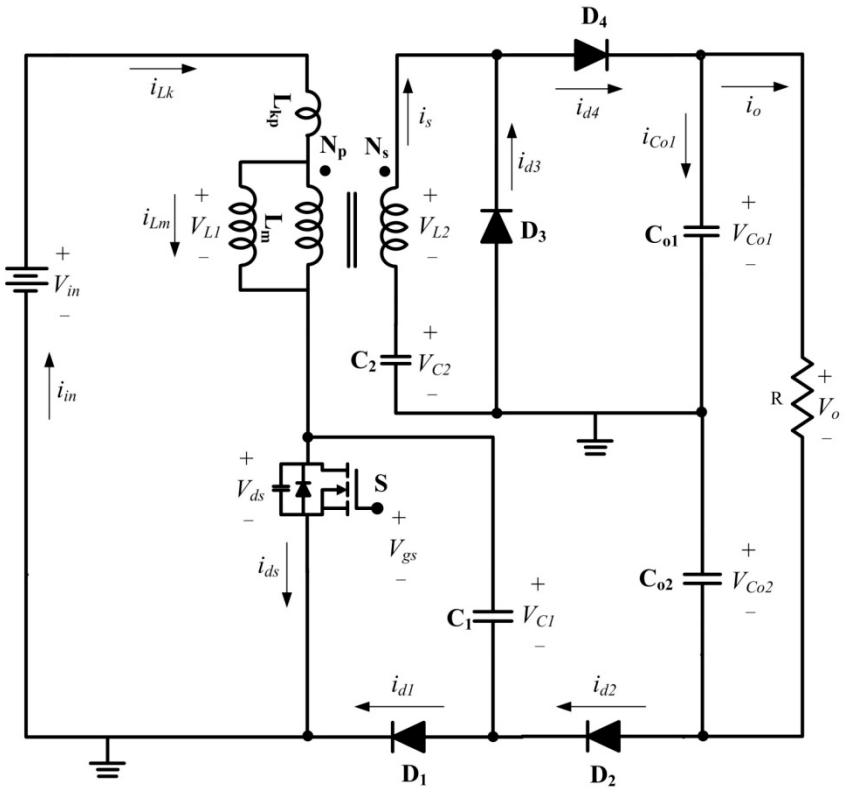

Fig. 1. Circuit configuration of the proposed converter

The CCM and DCM of the proposed converter operation are analyzed in detail.

2.1 CCM operation analysis

The key component of the current and voltage waveforms of the proposed converter at CCM is presented in Fig. 2. In CCM, the proposed converter has five operating modes that are classified based on the switch duty cycle.

Mode I [t_0, t_1]: During this period, power switch S is turned on. The equivalent circuit is illustrated in Fig. 3*a*. The clamp circuit diode D_1 and step-up circuit diode D_3 are forward-biased. The DC source supplies energy to the leakage magnet and transfers energy to the secondary side capacitor C_2 through the step-up circuit-isolated transformer. When diode D_3 is turned on, clamp circuit capacitor C_1 releases energy to the high voltage output capacitor C_{o2}. Therefore, the leakage magnet i_{Lk} and clamp circuit current i_{d2} increase linearly, whereas the secondary side leakage inductor current i_s decreases to zero. V_{c2} is approximately nV_{L1}, V_{c1} is equal to V_{co2}, and the voltage of parasitic capacitor on the main power switch is zero. This operating mode ends when the current of secondary side i_s is zero at $t = t_1$.

Mode II [t_1, t_2]: During this period, power switch S remains turned on. The equivalent circuit is indicated in Fig. 3*b*. The clamp circuit diode D_1 and step-up circuit diode D_4 are forward-biased. The DC source supplies energy to the leakage magnet L_{kp} and magnetizes inductor L_m. The secondary side capacitor C_2 and isolated transformer secondary coil discharge energy to the high voltage

 doi:10.20944/preprints201610.0074.v1

output capacitor C_{o1}, and the clamp circuit capacitor C_1 releases energy to the high voltage output capacitor C_{o2}. Thus, the leakage magnet i_{Lk} and magnetizing inductor current i_{Lm} increase linearly; and V_{c2} is approximately equal to $V_{co1} - nV_{L1}$, and V_{c1} is equal to V_{co2}, and voltage of parasitic capacitor on main power switch is zero. In this mode, the input source, magnetizing inductance, as well as the capacitor C_1 and capacitor C_2 energy, will be transmitted to the output capacitors Co_1 and Co_2. This operating mode ends when the power switch is turned off at $t = t_2$.

Mode III [t_2, t_3]: During this period, power switch S is turned off. The equivalent circuit is displayed in Fig. 4*a*. Clamp circuit diode D_1 and step-up circuit diode D_4 are forward-biased. The DC source and leakage magnet L_{kp} supply energy to the magnetizing inductor L_m and parasitic capacitor C_{ds} of the main power switch S. Secondary side capacitor C_2 and secondary coil current i_s increase linearly, output capacitors C_{o1} and C_{o2} provide energy to output loading, and voltage of parasitic capacitor on main power switch is equal to $V_{in} - V_{L1}$. This mode ends when the parasitic capacitor C_{ds} energy becomes fully charged.

Mode IV [t_3, t_4]: During this period, power switch S is turned off at $t = t_3$. The equivalent circuit is illustrated in Fig. 4*b*. Diodes D_1 and D_4 are forward-biased. Magnetizing inductor L_m and passive clamp circuit capacitor C_1 charge energy via leakage inductor L_k. Leakage inductor current i_{Lk} decreases quickly because the energy is recycled by capacitor C_1. Secondary coil energy and capacitor C_2 continuously discharge energy to the high voltage side capacitor C_{o1}, and voltage of parasitic capacitor on main power switch is equal to V_{c1}. This mode ends at $t = t_4$ until capacitor C_2 voltage is equal to the output capacitor C_{o1} voltage.

Mode V [t_4, t_5]: During this period, power switch S is turned off. The equivalent circuit is illustrated in Fig. 4*c*. D_1 and D_3 are forward biased. DC source V_{in} and magnetizing inductor L_m discharge energy to capacitor C_1, whereas capacitor C_2 charges energy via D_3 by secondary coil induced energy; voltage of parasitic capacitor on main power switch is equal to V_{c1}. Power switch S is turned on at the next period at $t = t_5$, during which this mode ends.

Preprints (www.preprints.org) | NOT PEER-REVIEWED | Posted: 18 October 2016 doi:10.20944/preprints201610.0074.v1

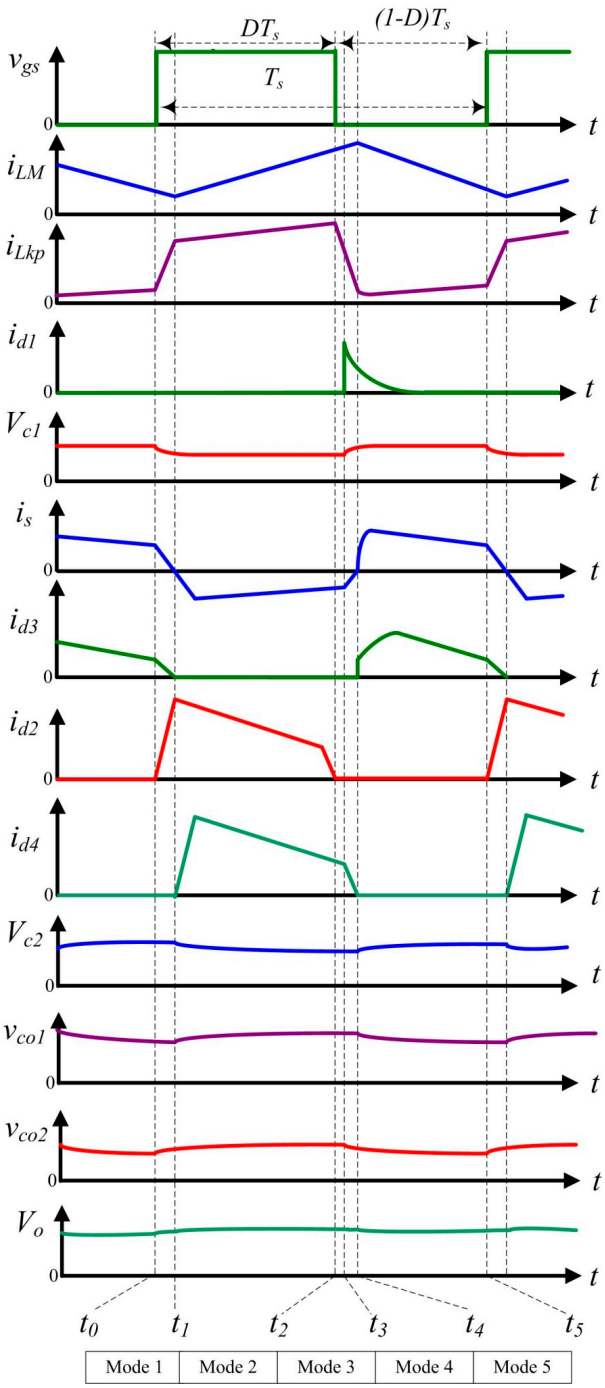

Fig. 2. Current and voltage waveforms of the key components of the proposed converter at CCM

Preprints (www.preprints.org) | NOT PEER-REVIEWED | Posted: 18 October 2016 doi:10.20944/preprints201610.0074.v1

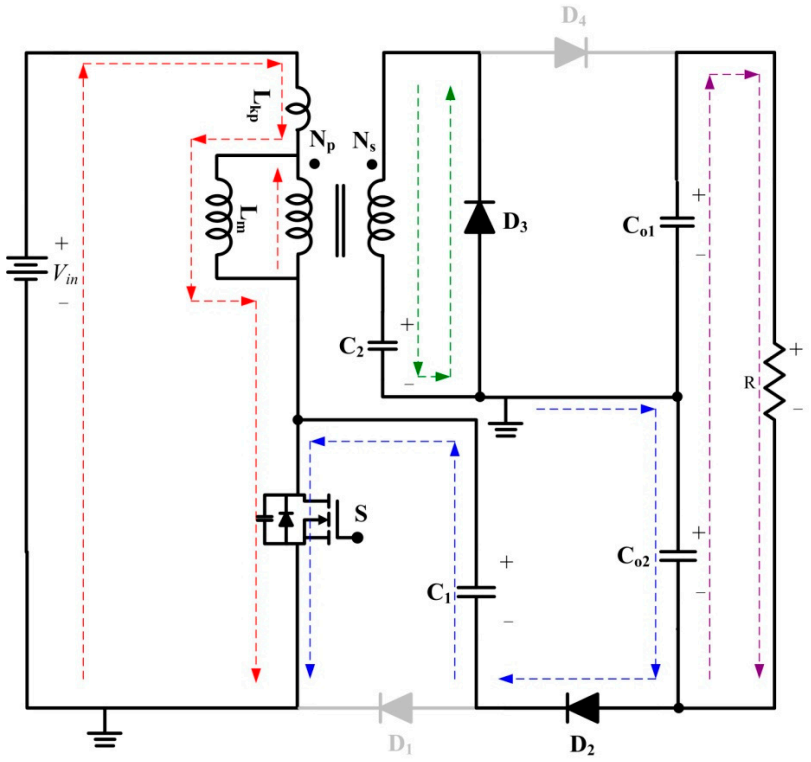

(a)

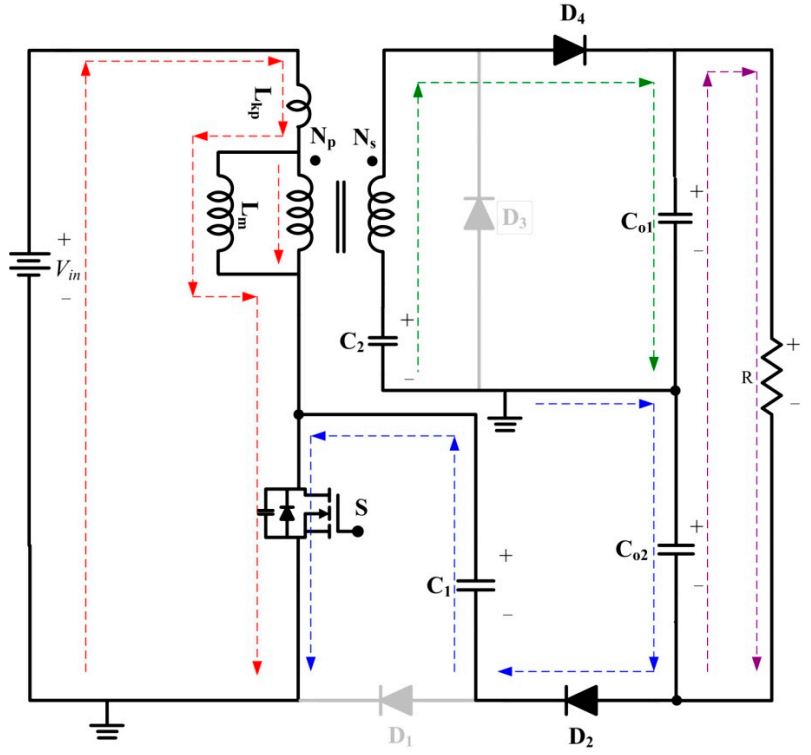

(b)

Fig. 3. Operating modes at CCM (switch turned on) during a switching period

a Mode I

b Mode II

Preprints (www.preprints.org) | NOT PEER-REVIEWED | Posted: 18 October 2016 doi:10.20944/preprints201610.0074.v1

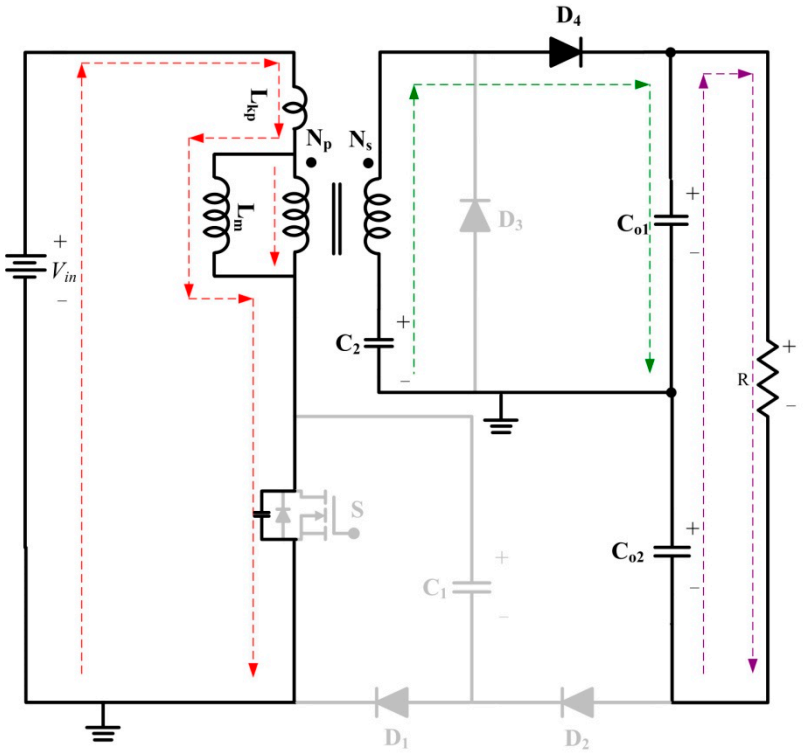

(a)

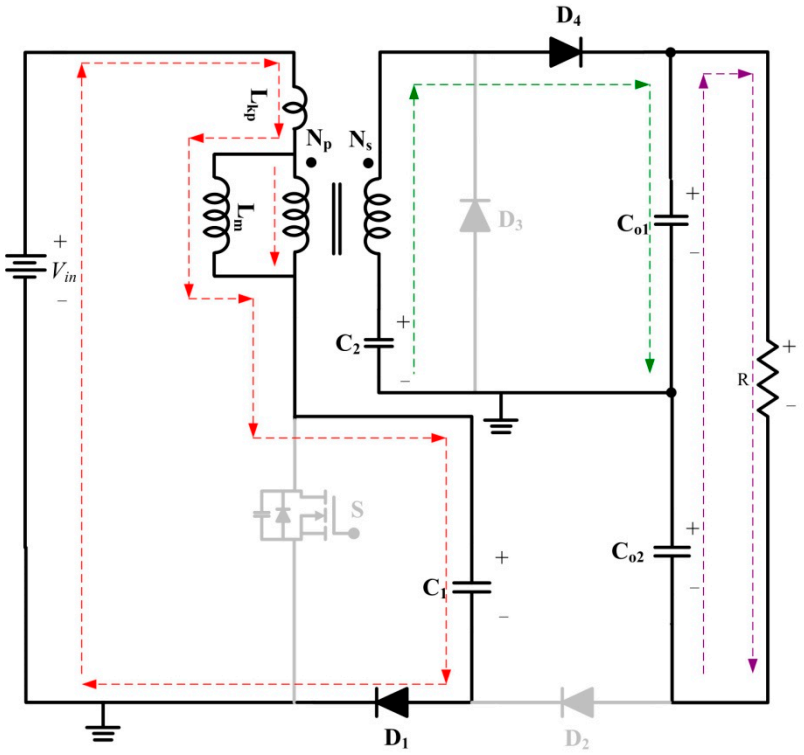

(b)

Preprints (www.preprints.org) | NOT PEER-REVIEWED | Posted: 18 October 2016 doi:10.20944/preprints201610.0074.v1

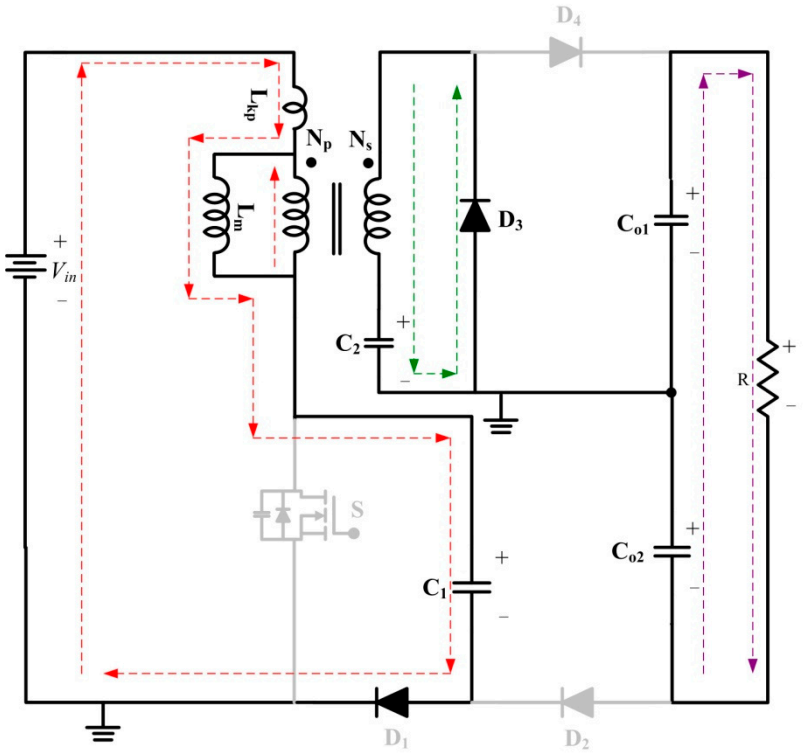

(c)

Fig. 4. Operating modes at CCM (switch turned off) during a switching period

a Mode III

b Mode IV

c Mode V

2.2 DCM operation analysis

In this section, the proposed circuit operation at DCM will be discussed. The leakage inductor L_k and parasitic capacitor of main power switch will not be discussed to simplify the analysis. The key component current and voltage waveforms are presented in Fig. 5. Fig. 6 presents the proposed circuit in modes I to III during operation.

Mode I [t_0, t_1]: Power switch S is turned on. The proposed converter equivalent circuit is shown in Fig. 6*a*. D_2 and D_4 are forward-biased. DC source V_{in} supplies energy to magnetizing inductor L_m, and the magnetizing inductor current i_{Lm} increases linearly. Secondary side capacitor C_2 and secondary coil discharge energy to capacitor C_{o1}. Passive clamp circuit capacitor C_1 then discharges energy to capacitor C_{o1}. Serial output capacitors C_{o1} and C_{o2} provide energy to output loading. This mode ends when power switch S is turned off at $t = t_1$.

Mode II [t_1, t_2]: Power switch S is turned off at this period. The proposed converter equivalent circuit is exhibited in Fig. 6*b*. D_1 and D_3 are forward-biased. DC source V_{in} and magnetizing inductor L_m supply energy to secondary side coil and capacitor C_1. The C_2 capacitor via D_3 charges energy via the secondary coil of the isolated transformer. This mode ends when the magnetizing inductor current i_{Lm} is equal to zero at $t = t_2$.

Mode III [t_2, t_3]: Power switch S is turned off at this period. The proposed converter equivalent circuit is illustrated in Fig. 6*c*. All the diodes are turned off and high voltage side-output capacitors C_{o1} and C_{o2} provide energy to output loading. This mode ends at $t = t_3$, and power switch S is turned on at the next period.

Preprints (www.preprints.org) | NOT PEER-REVIEWED | Posted: 18 October 2016 doi:10.20944/preprints201610.0074.v1

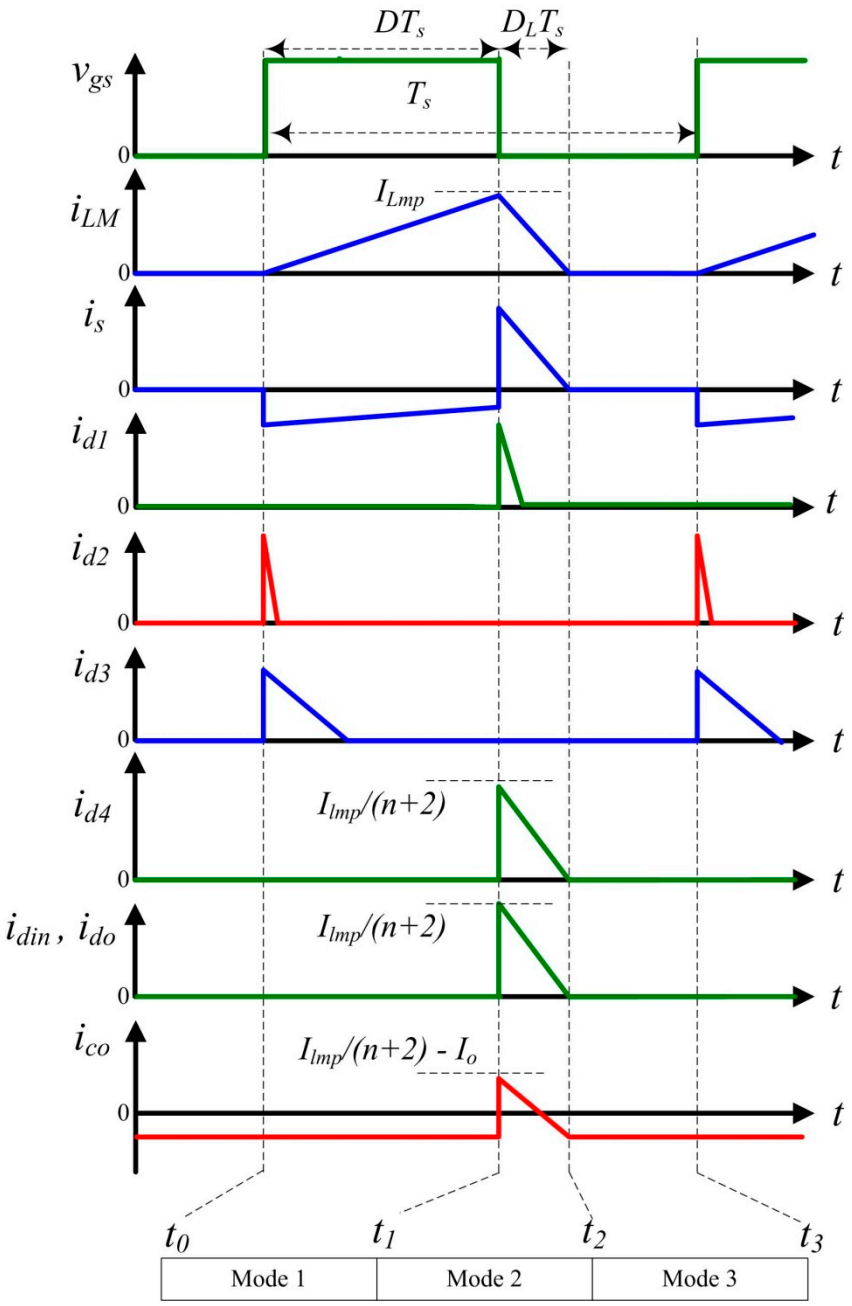

Fig. 5. Current and voltage waveforms of the key components of the proposed converter at DCM operation

Preprints (www.preprints.org) | NOT PEER-REVIEWED | Posted: 18 October 2016 doi:10.20944/preprints201610.0074.v1

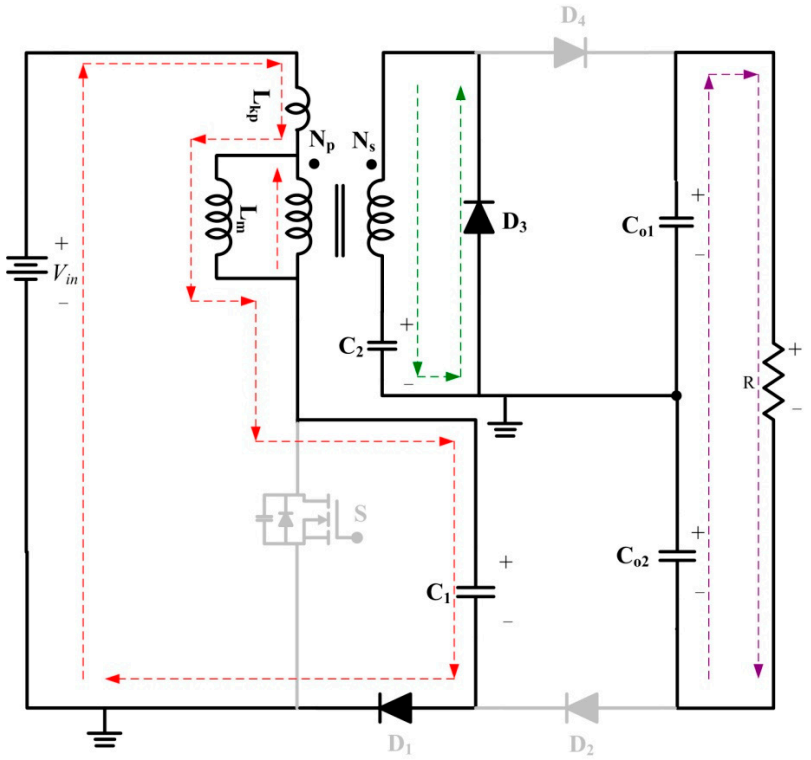

(a)

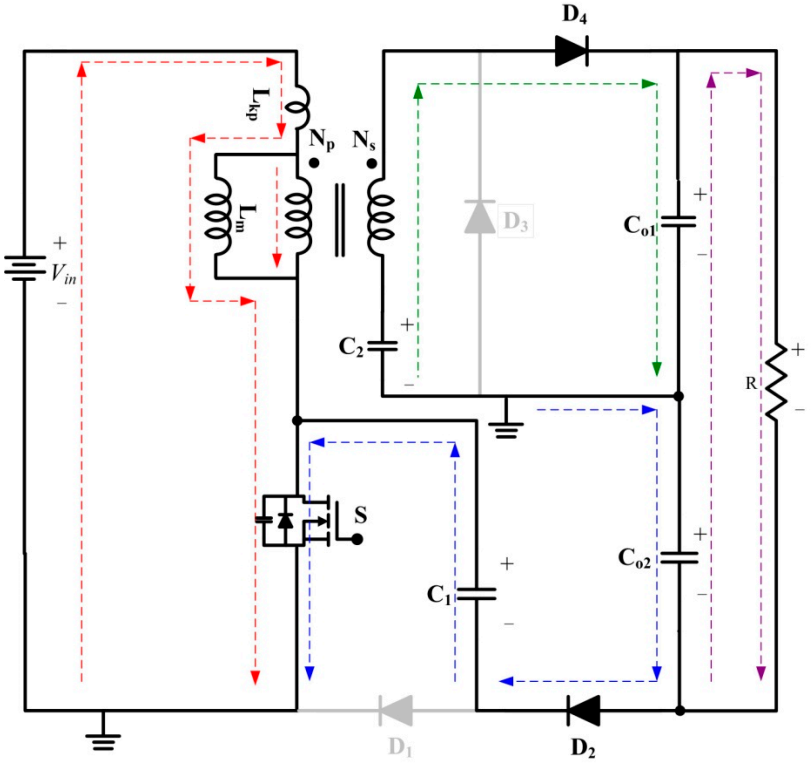

(b)

Preprints (www.preprints.org) | NOT PEER-REVIEWED | Posted: 18 October 2016 doi:10.20944/preprints201610.0074.v1

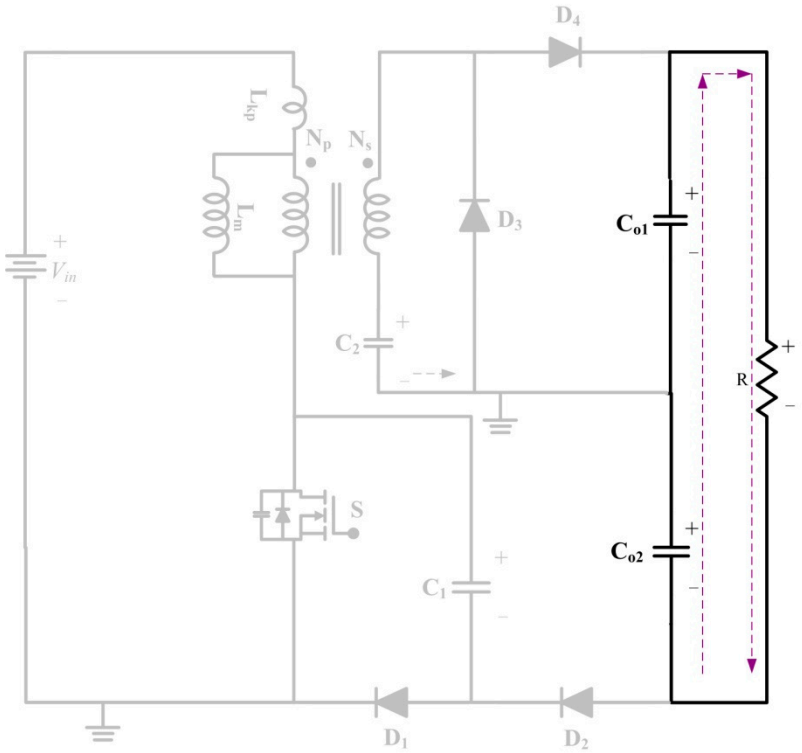

(c)

Fig. 6. Operating modes at DCM during a switching period

a Mode I
b Mode II
c Mode III

3. Steady-state Analysis

The steady-state analysis of the proposed converter is discussed in this section. The assumed condition equations of turn ratio and coupling coefficients *k* are defined as follows:

$$n = \frac{N_s}{N_p} \quad (1)$$

$$k = \frac{L_m}{L_m + L_k} \quad (2)$$

To simplify the steady-state analysis, any L_k value smaller than L_m is neglected, and coupling coefficient *k* should be equal to 1. Modes I, III, and IV are short and disregarded by one switching cycle. The time intervals of modes II and V are considered.

3.1 CCM operation analysis

V_{L1} and V_{L2} are across voltages at mode II. The following equations can be derived from Fig. 3*b*:

$$V_{L1}^{II} = V_{in} \quad (3)$$

$$V_{L2}^{II} = nV_{L1}^{II} = nV_{in} \quad (4)$$

Based on mode V, capacitor C_1 charges the DC source, and the primary coil and capacitor C_2 charge the secondary coil. The across voltages of V_{L1}^{II} and V_{L2}^{II} can be written as:

$$V_{L1}^{V} = V_{in} - V_{c1} \quad (5)$$

$$V_{L2}^{V} = -V_{c2} \quad (6)$$

According the volt-second balance principle, the voltage equations of N_p and N_s are expressed as:

$$\int_0^{DT_s} V_{L1}^{II} dt + \int_{DT_s}^{T_s} V_{L1}^{V} dt = 0 \quad (7)$$

$$\int_0^{DT_s} V_{L2}^{II} dt + \int_{DT_s}^{T_s} V_{L2}^{V} dt = 0 \quad (8)$$

By using (3) and (5) into (7), the stress voltage of N_p in a switching period can be obtained by:

$$V_{in}(DT_s) + (V_{in} - V_{c1})(1 - DT_s) = 0 \quad (9)$$

$$V_{c1} = V_{in}/(1 - D) \quad (10)$$

Preprints (www.preprints.org) | NOT PEER-REVIEWED | Posted: 18 October 2016 doi:10.20944/preprints201610.0074.v1

According to (4) and (6) to (8), stress voltage of N_s in a switching period can be arranged as:

$$nV_{in}(DT_s) + (-V_{c2})(1 - DT_s) = 0 \quad (11)$$

$$V_{c2} = nDV_{in}/(1 - D) \quad (12)$$

At mode II, capacitor C_1 releases energy to capacitor C_{o2}, and capacitor C_2 and the secondary coil release energy to capacitor C_{o1}. The across voltages of V_{co1}, V_{co2}, and V_o are derived by:

$$V_{co1} = V_{c2} + V_{L2}^{II} \quad (13)$$

$$V_{co2} = V_{c1} \quad (14)$$

$$V_o = V_{c1} + V_{c2} + V_{L2}^{II} \quad (15)$$

By substituting (12) and (4) into (13), and (10) into (14), the stress voltage of capacitors C_{o1} and C_{o2} can be rewritten as:

$$V_{co1} = nDV_{in}/(1 - D) + nV_{in} \quad (16)$$

$$V_{co2} = V_{in}/(1 - D) \quad (17)$$

Substituting (4), (10), and (12) to (15), the output voltage equations can be expressed as:

$$V_o = V_{in}/(1 - D) + nDV_{in}/(1 - D) + nV_{in}$$
$$= \frac{1+n}{1-D} V_{in} \quad (18)$$

The voltage gain can obtained as follows:

$$M_{CCM} = \frac{1+n}{1-D} \quad (19)$$

The use of voltage-clamped technology to reduce reverse-recovery current and switch-voltage stress are discussed in the literature [24].Circuit topology is the combination of an inductor and a transformer to increase the corresponding voltage gain. One additional inductor is a reduced reverse-current and one additional capacitor is a clamp voltage of the main power switch that can reduce switch-voltage stress. According to literature [24], voltage gain is $M_{CCM[24]} = \frac{1+n}{1-D}$. Comparisons of the voltage gains of the proposed converter and one presented in a previous study [24] are shown in Fig. 7. The voltage gain of the proposed converter is higher than that of the converter presented in [24] (see Fig. 7).

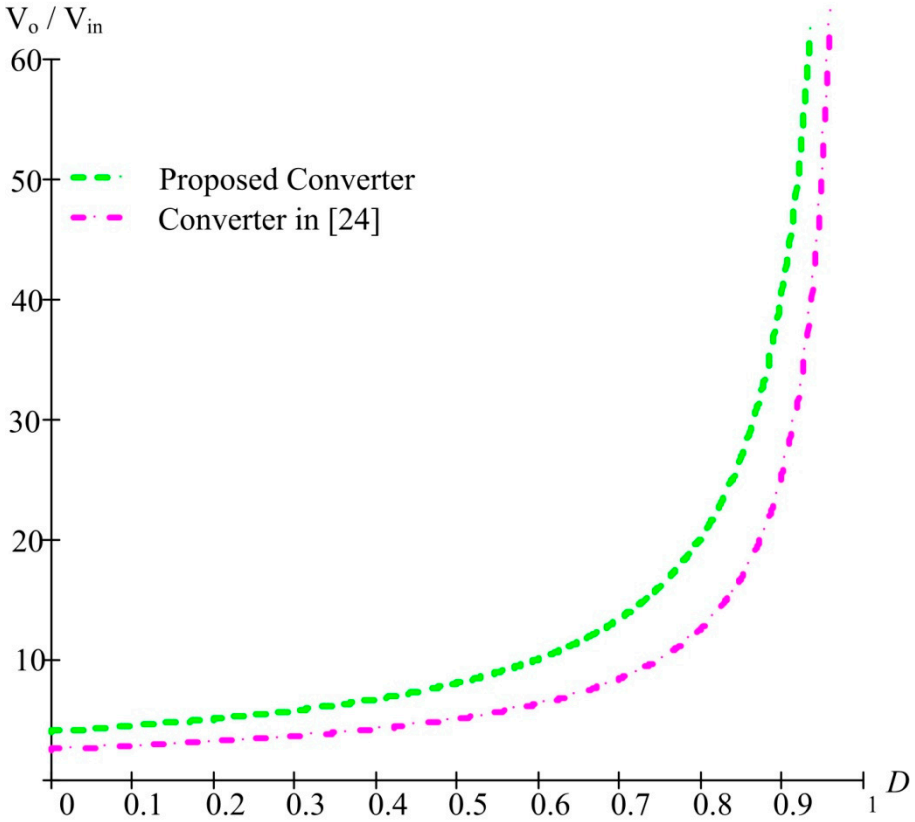

Fig. 7. Duty ratio versus voltage gain of the proposed converter compared with the converter in [24]; condition is CCM operation under $k = 1$ and $n = 3$

Preprints (www.preprints.org) | NOT PEER-REVIEWED | Posted: 18 October 2016 doi:10.20944/preprints201610.0074.v1

3.2 DCM operation analysis

Three modes have been discussed at DCM operation. Fig. 5 illustrates the key component current and voltage waveforms.

Mode I: During this period, the main power switch *S* is turned on and the magnetizing inductor charges the DC source. Fig. 6*a* presents the operation. The equation can be expressed as follows:

$$V_{L1}^{I} = V_{in} \quad (20)$$

$$V_{L2}^{I} = nV_{in} \quad (21)$$

The peak current of the magnetizing inductor can be defined as:

$$I_{Lmp} = \frac{V_{in}}{Lm} DT_s \quad (22)$$

The across voltages of C_1 and C_2 are given as:

$$V_{c2} = V_{co1} - V_{L2}^{I} \quad (23)$$

$$V_{c1} = V_{co2} \quad (24)$$

$$V_o = V_{c1} + V_{c2} + V_{L2}^{I} \quad (25)$$

Mode II: During this period, main power switch *S* is turned off, and the input voltage and magnetizing inductor energy discharge energy to capacitor C_1. Fig. 6*b* illustrates the operating mode.

$$V_{L1}^{II} = V_{in-}V_{c1} \quad (26)$$

$$V_{L2}^{II} = -V_{c2} \quad (27)$$

Fig. 6*c* presents mode III. The output capacitors C_{o1} and C_{o2} discharge energy to output loading.

$$V_{L1}^{III} = V_{L2}^{III} = 0 \quad (28)$$

Based on the volt-second balance principle, the steady state operation of an inductor in a DC-DC converter and net inductor voltage in a switching period must be zero.

$$\int_0^{DT_s} V_{L1}^{I} dt + \int_{DT_s}^{(D+D_L)T_s} V_{L1}^{II} dt + \int_{(D+D_L)T_s}^{T_s} V_{L1}^{III} dt = 0 \quad (29)$$

$$\int_0^{DT_s} V_{L2}^{I} dt + \int_{DT_s}^{(D+D_L)T_s} V_{L2}^{II} dt + \int_{(D+D_L)T_s}^{T_s} V_{L2}^{III} dt = 0 \quad (30)$$

From (20), (26), and (28) to (29); and (21), (27), and (28) to (30), the stress voltages of capacitors C_1 and C_2 are:

$$V_{c1} = \frac{D+D_L}{D_L} V_{in} \quad (31)$$

$$V_{c2} = \frac{D}{D_L} nV_{in} \quad (32)$$

Substituting (21), (31), and (32) to (25), the voltage gain of the proposed converter at DCM can be obtained using:

$$V_o = [(1+n)(1+\frac{D}{D_L})]\, V_{in} \quad (33)$$

$$D_L = \frac{(1+n)DV_{in}}{V_o-(1+n)V_{in}} \quad (34)$$

Based on Fig. 5, i_{co1} is the average current value of the output capacitor C_{o1}, and the average values of the I_{co} and I_{co1} can be calculated by:

$$I_{co} = I_{D4} - I_o \quad (35)$$

$$I_{co1} = \frac{1}{2} D_L \frac{I_{Lmp}}{1+n} - I_o \quad (36)$$

In the steady state, I_{co1} equals zero. (22), (34), and $I_{co1} = 0$ can be substituted to (36). Thus, (36) can be rewritten as:

$$\frac{1}{2(n+1)} \cdot \frac{(n+1)D^2 {V_{in}}^2 T_s}{[V_o-(1+n)V_{in}]\cdot Lm} = \frac{V_o}{R} \quad (37)$$

The time constant of magnetizing inductance is defined as:

$$\tau_{Lm} \overset{\text{def}}{=} \frac{Lm}{RT_s} \quad (38)$$

Substituting (38) with (37), the voltage gain can be obtained by:

$$M_{\text{DCM}} = \frac{V_o}{V_{in}} = \frac{1+n}{2} + \sqrt{\frac{(1+n)^2}{4} + \frac{D^2}{2\cdot\tau_{Lm}}} \quad (39)$$

3.3 Boundary operating condition between CCM and DCM

The voltage gain is equal at CCM and DCM when the proposed converter operation is in boundary condition mode. Based on the formulas (19) and (39), the time constant τ_{LmB} of the boundary-normalized magnetizing inductor can be written as:

$$\tau_{LmB} = \frac{D^2(1-D)^2}{2(1+n+nD)^2-(1+2n+n^2)(1-2D+D^2)} \quad (40)$$

Preprints (www.preprints.org) | NOT PEER-REVIEWED | Posted: 18 October 2016 doi:10.20944/preprints201610.0074.v1

Fig. 8 indicates that, if the curve of τ is lower than that of τ_{LmB}, then the proposed converter operation is in DCM. Otherwise, if the curve of τ is higher than that of τ_{LmB}, then the proposed converter operation is in CCM.

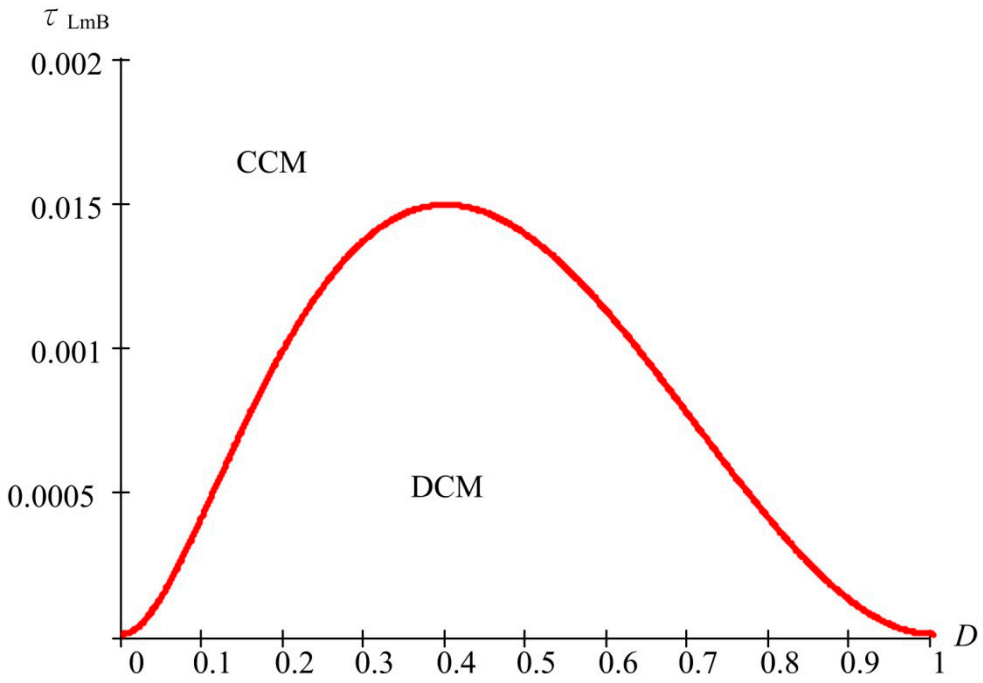

Fig. 8. Duty ratio versus τ_{LmB} at the boundary condition of the proposed converter under $n = 3$

4. Experimental Results of the Proposed Converter

A 150 W isolated converter was built in the laboratory to prove its effectiveness and performance. The input DC voltage was 24 V, and the output voltage was 200 V. The main power switch S selected had low conduction, low voltage stress components, and with a switch frequency of 50 kHz. The main specifications are presented in Table 1.

The experimental results can be divided into current and voltage waveform testing results. Fig. 9 illustrates the proposed converter current waveform of the key components at full load. The input voltage was 24 V, and the output power was 150 W. Fig. 9*a* presents the isolated transformer primary and secondary currents along with the drain to source voltage from the main power switch. Drain to source voltage of the main power switch was 0 V when the main switch was turned on, and when the primary current linearly increased, the peak current of the magnetizing inductor is $I_{Lmp} = \frac{V_{in}}{Lm} DT_s$. Otherwise, voltage of the main power switch was $V_{ds} = V_{in} + V_{L1}$ and current of the magnetizing inductor is $I_{Lmp} = \frac{V_{in}-V_{c1}}{Lm}(D_L)T_s$ until it decreased the current to zero when the main power switch was turned off. Fig. 9*b* presents the diode current versus V_{ds}. The waveforms of i_{d1} and i_{d2} illustrates that capacitor C_1 charges and discharges when the main switch is turned on and off, respectively. Capacitor C_1 releases energy through D_2 and the main power switch to output capacitor C_{o2}, and i_{d2} is the forward current when the main power switch is turned on. At the next period, capacitor C_1 was charged by magnetizing the inductor and input source. Moreover, the voltage of main power switch was clamped to V_{c1} through diode D_1. i_{d1} is the forward current when the main power switch is turned off. Fig. 9*c* illustrates that the waveforms of i_{d3} and i_{d4} reveals that capacitor C_2 charges energy to the secondary coil through D_3 and i_{d3} is the forward current when the main power switch is turned on. Otherwise, capacitor C_2 discharges energy to capacitor C_{o1} through D_4 and i_{d4} is the forward current when the main switch is turned off. Figs. 10*a* and 10*b* exhibit the measurements of the waveform of the capacitor voltages. Fig. 10*a* presents the measurements of the capacitor voltages of C_1 and C_2 that can satisfy formulas (10) and (12). Capacitor C_1 releases energy through D_2 and is charged via the input source and magnetizing inductor. Capacitor C_2 changed to secondary coil via diode D_3 and discharged energy to secondary coil and output capacitor C_{o1}

Preprints (www.preprints.org) | NOT PEER-REVIEWED | Posted: 18 October 2016 doi:10.20944/preprints201610.0074.v1

through diode D_4. Fig. 10*b* displays the measurements of the capacitor voltages of C_{o1} and C_{o2}. V_{co1}, V_{co2}, and V_o test results are satisfied by (16), (17), and (18). Voltage of capacitor C_{o2} is equal to voltage of capacitor C_1. Voltage of capacitor C_{o1} is equal to V_{c2}+V_{L2}^{II}. Output voltage is sum to V_{co1} and V_{co2}. Finally, the measured efficiency of the proposed converter is within 30–150 W (see Fig. 11), and the maximum efficiency is 95.1% at 60 W.

Table 1. Specifications of the proposed converter

Parameter	Symbol	Value
Input voltage	V_{in}	24 V
Output voltage	V_o	200 V
Maximum output power	P_{max}	150 W
Main switch frequency	f_s	50 kHz
Main switch	S	IXTH130N10T
Diodes	D_1–D_4	DSEI 30–10 A
Capacitors	C_1, C_2, C_{o2}	100 μF/100 V
Capacitor	C_{o1}	220 μF/200 V
Turn ratio	N_p/N_s	1:3
Isolated transformer	T	$L_m = 33$ μH, $L_k = 0.26$ μH
Coupling coefficient	K	0.992

Preprints (www.preprints.org) | NOT PEER-REVIEWED | Posted: 18 October 2016 doi:10.20944/preprints201610.0074.v1

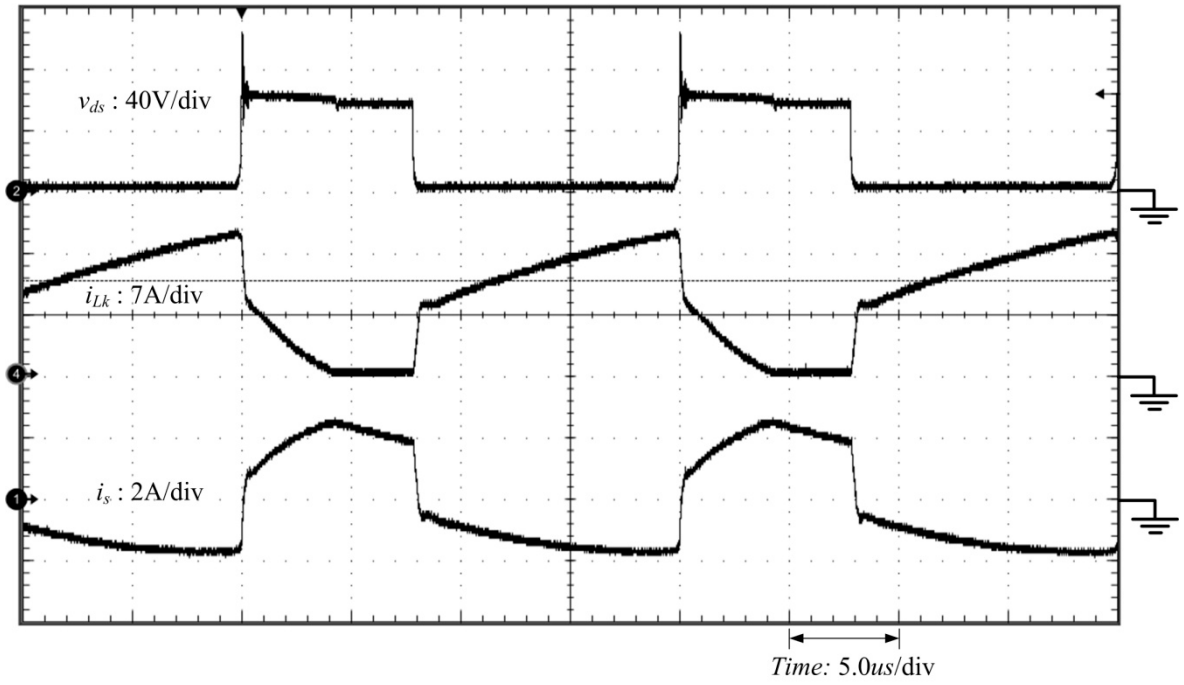

(a)

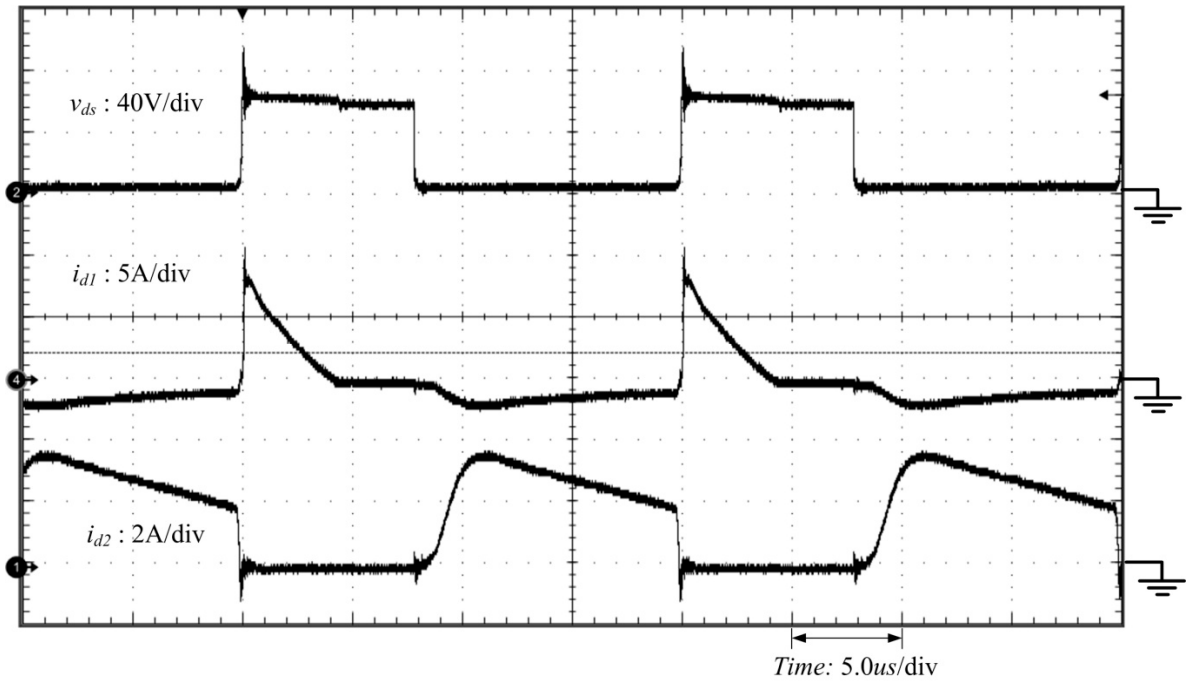

(b)

Preprints (www.preprints.org) | NOT PEER-REVIEWED | Posted: 18 October 2016 doi:10.20944/preprints201610.0074.v1

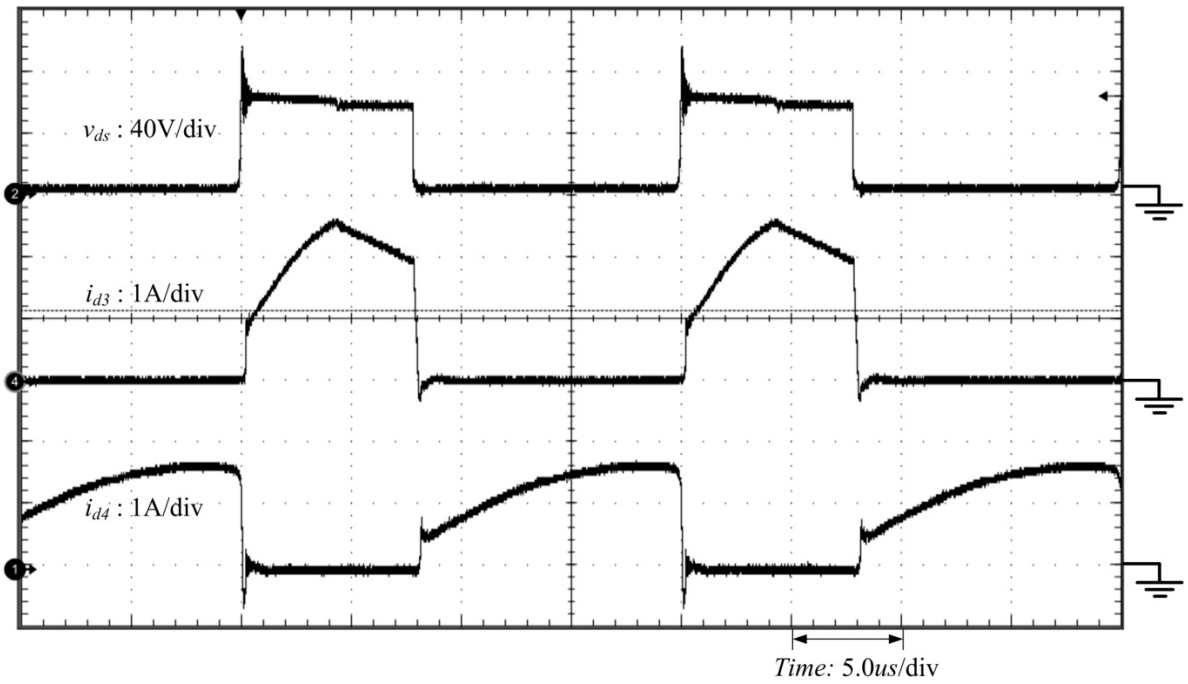

(c)

Fig. 9. Experimental current waveform under full-load P_o = 150 W
a Measured waveforms of v_{ds}, i_{Lk}, and i_s
b Measured waveforms of v_{ds}, i_{d1}, and i_{d2}
c Measured waveforms of v_{ds}, i_{d3}, and i_{d4}

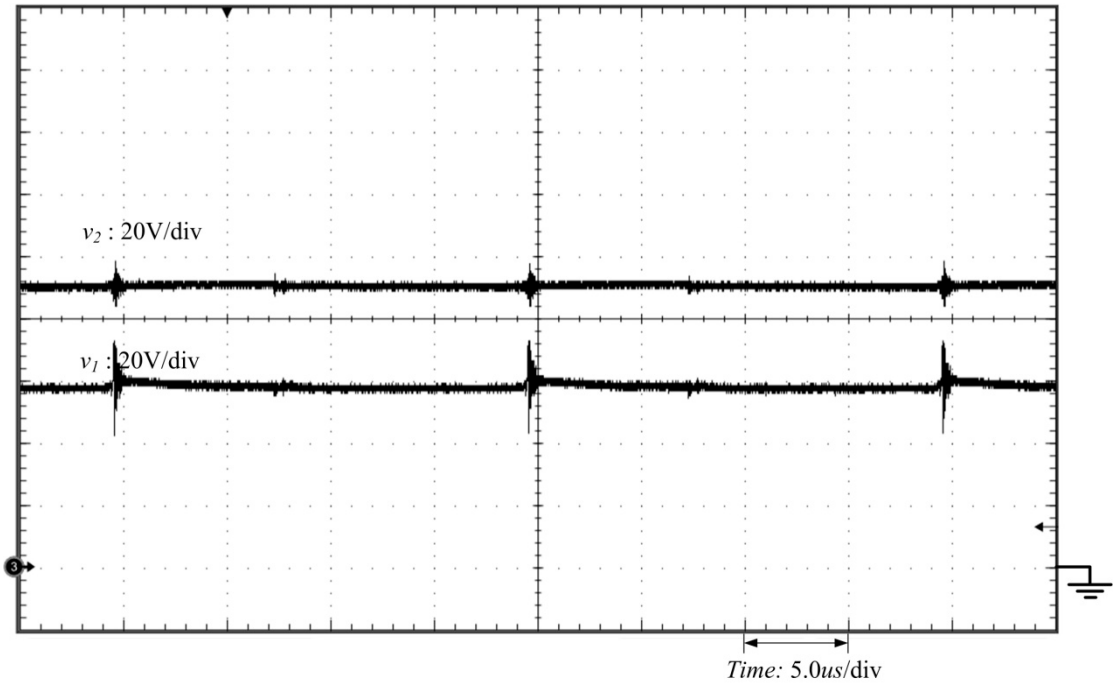

(a)

Preprints (www.preprints.org) | NOT PEER-REVIEWED | Posted: 18 October 2016 doi:10.20944/preprints201610.0074.v1

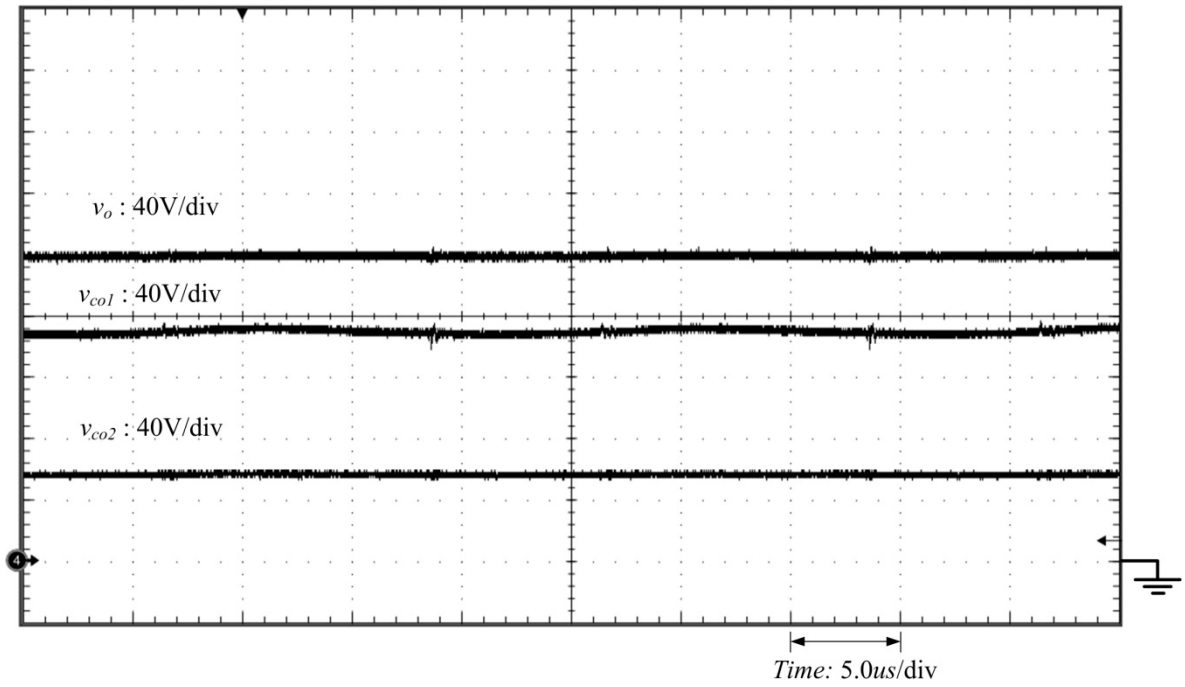

(b)

Fig. 10. Experimental voltage waveform under full-load $P_o = 150\ W$
a Measured waveforms of v_1, v_2, and v_3
b Measured waveforms of v_{co1}, v_{co2}, and v_o

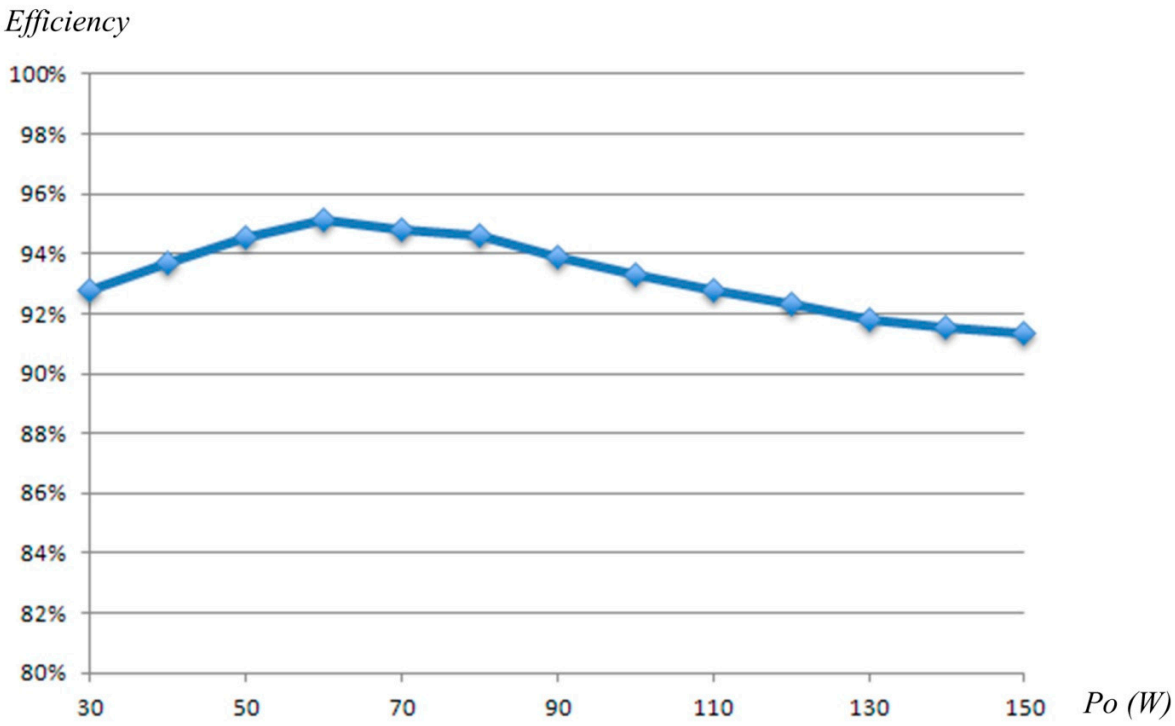

Fig. 11. Efficiency of the proposed converter

5. Conclusions

In this study, a high step-up voltage circuit was successfully designed and fabricated in the laboratory. The proposed converter uses an isolated transformer and a clamp capacitor circuit to achieve high voltage gain. The clamp capacitor circuit can be used to recycle the energy of the

 doi:10.20944/preprints201610.0074.v1

primary leakage inductor and reduce the voltage spike of the main power switch when the power switch is turned off. Thus, low voltage stress and conducting resistance $R_{ds(on)}$ component can be selected to ensure reduced switch loss on the power switch, thereby improving the efficiency of the proposed converter. Finally, a full power of a 150 W high step-up converter with an input voltage of 24 V and output voltage of 200 V was achieved. The experimental results demonstrated high efficiency of the proposed converter, with peak efficiency of 95.1%. In addition, the voltage stress on the main power switch is clamped at 50 V.

Supplementary

Conflicts of Interest: State any potential conflicts of interest here or "The authors declare no conflict of interest".

References

1. UNFCCC., 'Paris Agreement' (Publisher, 2015), pp. 1-2
2. N. Femia, G. Petrone, G. Spagnuolo and M. Vitelli, "A technique for improving P&O MPPT performances of double-stage grid-connected photovoltaic systems" IEEE Trans. on Industrial Electronics, Vol. 56, No. 11, pp. 4473-4482, Nov. 2009.
3. B. Q. Liu, F. Zhuo, Y. X. Zhu and H. Yi, "System operation and energy management of a renewable energy-based DC micro-grid for high penetration depth application" IEEE Trans. on Smart Grid, Vol. 6, No. 3, pp. 1147-1155, May. 2015.
4. Y. P. Hsieh, J. F. Chen, T. J. Liang and L. S. Yang, "Novel high step-up DC-DC converter for distributed generation system" IEEE Trans. on Industrial Electronics, Vol. 60, No. 4, pp. 1473-1482, Apr. 2013.
5. Y. P. Hsieh, J. F. Chen, T. J. Liang and L. S. Yang, "Novel high step-up DC-DC converter with coupled-inductor and switched-capacitor techniques for a sustainable energy system" IEEE Trans. on Power Electronics, Vol. 26, No. 26, pp. 3481-3490, Dec. 2011.
6. J. M. Carrasco, L. G. Franquelo, J. T. Bialasiewicz, E. Galvan, R. C. Portillo-Guisado, M. A. M. Prats, J. I. Leon and N. Moreno-Alfonso, "Power-electronic systems for the grid integration of renewable energy source: a survey" IEEE Trans. on Industrial Electronics, Vol. 53, No. 4, pp. 1002-1016, June. 2006.
7. M. Liserre, T. Sauter and J. Y. Hung, "Future energy systems: integrating renewable energy source into the smart power grid through industrial electronics" IEEE Trans. on Industrial Electronics, Vol. 4, No. 1, pp. 18-37, Mar. 2010.
8. W. H. Li, X. D. Lv, Y. Deng, J. Liu and X. N. He, "A review of non-isolated high step-up DC-DC converters in renewable energy applications" IEEE Applied Power Electronics Conference and Exposition, pp. 364-369, 2009.
9. F. Li and H. C. Liu, "Novel high step-up DC-DC converter with an active coupled-inductor network for a sustainable energy system" IEEE Trans. on Power Electronics, Vol. 30, No. 12, pp. 6476-6482, Dec. 2015.
10. R. J. Wai and R. Y. Duan, "High step-up converter with coupled-inductor" IEEE Trans. on Power Electronics, Vol. 20, No. 5, pp. 1025-1035, Sep. 2005.
11. Y. P. Hsieh, J. F. Chen, L. S. Yang, C. Y. Wu and W. S. Liu, "High-conversion-ratio bidirectional DC-DC converter with coupled inductor" IEEE Trans. on Industrial Electronics, Vol. 61, No. 1, pp. 210-222, Jan. 2014.
12. R. Y. Duan and J. D. Lee, "High-efficiency bidirectional DC-DC converter with coupled inductor" IET Power Electronics, Vol. 5, No. 1, pp. 115-123, Jan. 2012.
13. Y. P. Hsieh, J. F. Chen, T. J. Liang and L. S. Yang, "Novel high step up DC-DC converter with coupled-inductor and switched-capacitor techniques" IEEE Trans. on Industrial Electronics, Vol. 59, No. 2, pp. 998-1007, Feb. 2012.
14. B. Axelrod, Y. Beck and Y. Berkovich, "High step-up DC-DC converter based on the switched-coupled-inductor boost converter and diode-capacitor multiplier: steady state and dynamics" IET Power Electronics, Vol. 8, No. 8, pp. 1420-1428, Apr. 2015.
15. G. Wu, X. B. Ruan and Z. H. Ye, "Nonisolated High Step-up DC-DC converters adopting switched-capacitor cell" IEEE Trans. on Industrial Electronics, Vol. 62, No. 1, pp. 383-393, Jan. 2015.

16. J. H. Lee, T. J. Liang and J. F. Chen, "Isolated coupled-inductor-integrated DC–DC converter with nondissipative snubber for solar energy applications" IEEE Trans. on Industrial Electronics, Vol. 61, No. 7, pp. 3337-3348, Jul. 2014.
17. T. J. Liang, J. H. Lee, S. M. Chen, J. F. Chen, and L. S. Yang, "Novel isolated high step-up DC-DC converter with voltage lift" IEEE Trans. on Power Electronics, Vol. 60, No. 4, pp. 1483-1491, Apr. 2013.
18. M. Delshad and H. Farzanehfard, "High step-up zero-voltage switching current-fed isolated pulse width modulation DC-DC converter" IET Power Electronics, Vol. 4, No. 3, pp. 316-322, Mac. 2011.
19. T. J. Liang and J. H. Lee, "Novel high-conversion-ratio high-efficiency isolated bidirectional DC-DC converter" IEEE Trans. on Industrial Electronics, Vol. 62, No. 7, pp. 4492-4503, Jul. 2015.
20. S. Inoue and H. Akagi, "A bidirectional DC-DC converter for an energy storage system with galvanic isolation" IEEE Trans. on Power Electronics, Vol. 22, No. 6, pp. 2299-2306, Nov. 2007.
21. Y. Zhao, W. Li, Y. Deng and X. He, "High step-up boost converter with passive lossless clamp circuit for non-isolated high step-up applications" IET Power Electronics, Vol. 4, No. 8, pp. 851-859, Sep. 2011.
22. T. F. Wu, Y. S. Lai, J. C. Hung and Y. M. Chen, "Boost converter with coupled inductors and buck-boost type of active clamp" IEEE Trans. on Industrial Electronics, Vol. 55, No. 1, pp. 154-162, Jan. 2008.
23. H. Mao, S. Q. Deng, J. Abu-Qahouq and I. Batarseh, "Active-clamp snubbers for isolated half-bridge DC-DC converters" IEEE Trans. on Power Electronics, Vol. 20, No. 6, pp. 1294-1302, Nov. 2005.
24. R. J. Wai, L. W. Liu and R. Y. Duan, "High-efficiency voltage-clamped DC-DC converter with reduced reverse-recovery current and switch-Voltage stress" IEEE Trans. on Industrial Electronics, Vol. 53, No. 1, pp. 272-280, Feb. 2006.
25. K. I. Hwu and Y. T. Yau, "Voltage-boosting converter based on charge pump and coupling inductor with passive voltage clamping" IEEE Trans. on Industrial Electronics, Vol. 57, No. 5, pp. 1719-1727, May. 2010..